Deep Time-Frequency Representation and Progressive Decision Fusion for ECG Classification

Jing Zhang[a], Jing Tian[a], Yang Cao[b], Yuxiang Yang[c,*], Xiaobin Xu[a,*]

[a]*School of Automation, Hangzhou Dianzi University*
[b]*Department of Automation, University of Science and Technology of China*
[c]*School of Electronics and Information, Hangzhou Dianzi University*

Abstract

Early recognition of abnormal rhythms in ECG signals is crucial for monitoring and diagnosing patients' cardiac conditions, increasing the success rate of the treatment. Classifying abnormal rhythms into exact categories is very challenging due to the broad taxonomy of rhythms, noises and lack of large-scale real-world annotated data. Different from previous methods that utilize hand-crafted features or learn features from the original signal domain, we propose a novel ECG classification method by learning deep time-frequency representation and progressive decision fusion at different temporal scales in an end-to-end manner. First, the ECG wave signal is transformed into the time-frequency domain by using the Short-Time Fourier Transform. Next, several scale-specific deep convolutional neural networks are trained on ECG samples of a specific length. Finally, a progressive online decision fusion method is proposed to fuse decisions from the scale-specific models into a more accurate and stable one. Extensive experiments on both synthetic and real-world ECG datasets demonstrate the effectiveness and efficiency of the proposed method.

Keywords:

Decision-making, Electrocardiography, Fourier transforms, Neural networks

*Corresponding author
Email addresses: yyx@hdu.edu.cn (Yuxiang Yang), xuxiaobin1980@163.com (Xiaobin Xu)

1. Introduction

Electrocardiogram (ECG), which records the electrical depolarization-repolarization patterns of the heart's electrical activity in the cardiac cycle, is widely used for monitoring or diagnosing patients' cardiac conditions [1, 2, 3]. The diagnosis is usually made by well-trained and experienced cardiologists, which is laborious and expensive. Therefore, automatic monitoring and diagnosing systems are in great demand in clinics, community medical centers, and home health care programs. Although advances have been made in ECG filtering, detection and classification in the past decades [3, 4, 5, 6], it is still challenging for efficient and accurate ECG classification due to noises, various types of symptoms, and diversity between patients.

Before classification, a pre-processing filtering step is usually needed to remove a variety of noises from the ECG signal, including the power-line interference, baseline wander, muscle contraction noise, *etc.* Traditional approaches like low-pass filters and filter banks can reduce noise but may also lead some artifacts [7]. Combining signal modeling and filtering together may alleviate this problem, but it is limited to a single type noise [8, 9]. Recently, different noise removal methods based on wavelet transform has been proposed by leveraging its superiority in multi-resolution signal analysis [10, 11, 12]. For instance, S. Poungponsri and X.H. Yu proposed a novel adaptive filtering approach based on wavelet transform and artificial neural networks that can efficiently removal different types of noises [12].

For ECG classification, classical methods usually consist of two sequential modules: feature extraction and classifier training. Hand-crafted features are extracted in the time domain or frequency domain, including amplitudes, intervals, and higher-order statistics, *etc.* Various methods have been proposed such as filter banks [13], Kalman filter [14], Principal Component Analysis (PCA)[15, 16], and wavelet transform (WT) [17, 18, 19, 4, 20]. Classifier models including Hidden Markov Models (HMM), Support Vector Machines (SVM) [21], Artificial Neural Networks (ANN) [4, 5, 17, 22, 6, 23], and mixture-of-experts method [24] have also been studied. Among them, a large number of methods are based on artificial neural networks due to its better modeling capacity. For example, L.Y. Shyu *et al.* propose a novel method

2

for detecting Ventricular Premature Contraction (VPC) using the wavelet transform and fuzzy neural network [4]. By using the wavelet transform for QRS detection and VPC classification, their method has less computational complexity. I. Guler and E.D. Ubeyli propose to use a combined neural network model for ECG beat classification [5]. Statistical features based on discrete wavelet transform are extracted and used as the input of first level networks. Then, sequential networks were trained using the outputs of the previous level networks as input. Unlike previous methods, T. Ince *et al.* propose a new method that uses a robust and generic ANN architecture and trains a patient-specific model with morphological wavelet transform features and temporal features for each patient [17]. Besides, some approaches have been proposed by combining several hand-crafted features to provide enhanced performance [25, 26]. Despite their usefulness, these methods have some common drawbacks: 1) the hand-crafted features rely on domain knowledge of experts and should be designed and tested carefully; 2) the classifier should have appropriate modeling capacity of such features; 2) The types of ECG signals are usually limited.

In the past few years, deep neural networks (DNN) have been widely used in many research fields and achieve remarkable performance. Recently, S. Kiranyaz *et al.* propose a 1-D convolutional neural network (CNN) for patient-specific ECG classification [3]. They design a simple but effective network architecture and utilize 1-D convolutions to processing the ECG wave signal directly. G. Clifford *et al.* organized the PhysioNet/Computing in Cardiology Challenge 2017 for AF rhythm classification from a short single lead ECG recording. A large number of real-world ECG samples from patients are collected and annotated. It facilitates research on the challenging AF classification problem. Both hand-crafted feature-based methods and deep learning-based methods have been proposed [27, 28, 29]. For example, S. Hong *et al.* propose an ensemble classifier based method by combining expert features and deep features [27]. T. Teijeiro *et al.* propose a combined two classifiers based method, *i.e.*, the first classifier evaluates the record globally using aggregated values for a set of high-level and clinically meaningful features, and the second classifier utilizes a Recurrent Neural Network fed with the individual features for each detected heartbeat [29]. M. Zabihi *et al.* propose a hand-crafted feature extraction and selection method based on a ran-

dom forest classifier [28].

In this paper, we propose a novel deep CNN based method for ECG classification by learning deep time-frequency representation and progressive decision fusion at different temporal scales in an end-to-end manner. Different from previous methods, 1) We first transform the original ECG signal into the time-frequency domain by Short-Time Fourier Transform (STFT). 2) Then, the time-frequency characteristics at different scales are learned by several scale-specific CNNs with 2-D convolutions. 3) Finally, we propose an online decision fusion method to fuse past and current decisions from different models into a more accurate one. We conducted extensive experiments on a synthetic ECG dataset consisting of 20 types of ECG signals and a real-world ECG dataset to validate the effectiveness of the proposed methods. The experimental results demonstrate its superiority over representative state-of-the-art methods.

2. Problem formulation

Given a set of ECG signals and their corresponding labels, the target of a classification method is to predict their labels correctly. As depicted in Section 1, it usually consists of two sequential modules: feature extraction and classifier training. Once the classifier is obtained, it can be used for unseen samples prediction, $i.e.$, testing phase. Mathematically, we denote the set of ECG wave signals as:

$$X = \{(x_i, y_i) \,|\, i \in \Lambda\}, \tag{1}$$

where x_i is the ith sequence with N samples : $x_i = [x_i(0), x_i(1), ..., x_i(N-1)]^T \in R^N$. $y_i \in \{0, .., C-1\}$ is the category of x_i, and C is the number of total categories. Λ is the index set of all samples. The feature extraction can be described as follows:

$$f_i = f(x_i, \theta_f), \tag{2}$$

where $f_i \in R^M$ is the corresponding feature representation of signal x_i. Usually, the feature vector f_i is more compact than the original signal x_i, $i.e.$, $M \ll N$. $f(\cdot, \theta_f)$ is a mapping function from the original signal space to the feature space, and θ_f is the parameters associated with the mapping $f(\cdot)$. It is usually determined according to
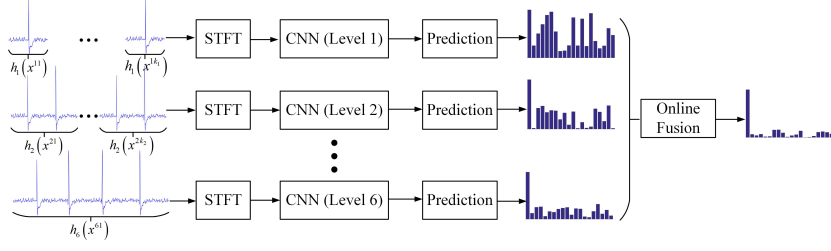
4

Figure 1: The pipeline of the proposed method for ECG classification.

domain knowledge of experts and cross-validation. Given the feature representation, a classifier $g\left(\cdot, \theta_g\right)$ predicts its category as follows:

$$c_i = g\left(f\left(x_i, \theta_f\right), \theta_g\right), \tag{3}$$

where θ_g is the parameters associated with the classifier $g\left(\cdot\right)$. $c_i \in \{0, .., C-1\}$ is the prediction. The frequently-used classifiers include SVM [21], ANN [22, 6, 23], Random Forest, Deep CNN [3], *etc*. Given the training samples, the training of a classifier can be formulated as an optimization problem of its parameter θ_g as follows:

$$\theta_g^* = \arg\min_{\theta_g} \sum_{i \in \Lambda_T} L\left(g\left(f\left(x_i, \theta_f\right), \theta_g\right), y_i\right), \tag{4}$$

where Λ_T is the index set of training samples. $L\left(\cdot\right)$ is a loss function which depicts the loss of assigning a prediction category c_i for a sample x_i with label y_i, *e.g.*, margin loss in SVM model and cross-entropy loss in models of ANN or Random Forest.

For deep neural networks models, feature extraction (learning) and classifier training are integrated together in the neural network architecture as an end-to-end model. The parameters are optimized for training samples by using the error back propagation algorithm. Mathematically, it can be formulated as:

$$\theta_h^* = \arg\min_{\theta_h} \sum_{i \in \Lambda_T} L\left(h\left(x_i, \theta_h\right), y_i\right), \tag{5}$$

where $h\left(\cdot, \theta_h\right)$ is the deep neural networks model with parameters θ_h. For a modern deep neural networks architecture, *e.g.*, Deep CNN, it usually consists of many sequential layers like convolutional layers, pooling layer, nonlinear activation layer, and fully connected layer, *etc*. Therefore, $h\left(\cdot, \theta_h\right)$ is a nonlinear mapping function with
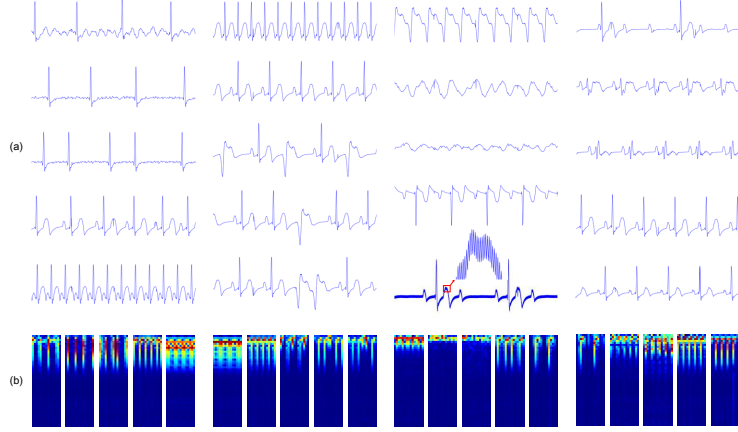
Figure 2: (a) Exemplar original ECG wave signals from each category. (b) Spectrograms of (a) using Short-Time Fourier Transform.

strong representation capacity and maps the original high-dimension input data to a low-dimension feature space, where features are more discriminative and compact.

3. The proposed approach

3.1. Short-Time Fourier Transform

Although wave signals in the original time domain can be used as input of DNN to learn features, a time-frequency representation calculated within a short-window may be a better choice [30]. Inspired by the work in speech recognition areas [31], where they show spectrogram features of speech are superior to Mel Frequency Cepstrum Coefficient (MFCC) with DNN, we first transform the original ECG wave signal into the time-frequency domain by using Short-Time Fourier Transform to obtain the ECG spectrogram representation. Mathematically, it can be described as follows:

$$s_i\left(k, m\right) = \sum_{n=0}^{N-1} x_i\left(n\right) w\left(m - n\right) e^{-j\frac{2\pi}{N}kn}, \tag{6}$$

where $w(\cdot)$ is the window function, $e.g.$, Hamming window. $s_i\left(k, m\right)$ is the two-dimension spectrogram of x_i. Figure 2 shows some examples of spectrograms.

Table 1: The proposed network architectures for ECG classification.

Network	Type	Input Size	Channels	Filter	Pad	stride
	Conv1	1x32x4	32	3x3	1	1
	Pool1	32x32x4	-	4x1	0	(4,1)
	Conv2	32x8x4	32	3x3	1	1
	Pool2	32x8x4	-	4x2	0	(4,2)
Proposed Network ($h1$)	Fc3	32x2x2	64	-	-	-
	Fc4	64x1x1	20	-	-	-
	Params			**18,976**		
	Complexity[1]			$3.5x10^5$		
	Conv1	1x1x512	32	1x15	(0,7)	(1,6)
	Conv2	32x1x86	16	1x15	(0,7)	(1,6)
	Conv3	16x1x15	16	1x15	(0,7)	(1,6)
Network in [3]	Pool3	16x1x3	-	1x3	0	1
	Fc4	16x1x1	10	-	-	-
	Fc5	10x1x1	20	-	-	-
	Params			**12,360**		
	Complexity			$1.7x10^5$		

3.2. Architecture of the proposed CNN

Since we use the two-dimension spectrogram as input, we design a deep CNN architecture that involves 2-D convolutions. Specifically, the proposed architecture consists of 3 convolutional layers and 2 fully-connected layers. There is a max-pooling layer and a ReLU layer after the first two convolutional layers and a max-pooling layer after the last convolutional layer, respectively. Details are shown in Table 1. As can be seen, it is quite light-weight with 18,976 parameters and 3.5×10^5 FLOPs. We also present the network architecture in [3] as a comparison. Filter sizes and strides are adapted to the data length used in this paper. It can be seen that the proposed network has a comparable amount of parameters and computational cost with the one in [3]. As will be shown in Section 4, the proposed method is computationally efficient and achieves a real-time performance even in an embedded device.

With the spectrogram s_i as input, the CNN model predicts a probability vector $p_i = h(s_i, \theta_h) \in R^C$ subjected to $\sum_{c=0}^{C-1} p_{ic} = 1$ and $p_{ic} \geq 0$. Then the model parameter θ_h can be learned by minimizing the cross-entropy loss as follows:

$$
\begin{aligned}
\theta_h^* &= \arg\min_{\theta_h} \sum_{i \in \Lambda_T} L\left(h\left(s_i, \theta_h\right), y_i\right) \\
&= \arg\min_{\theta_h} - \sum_{i \in \Lambda_T} \sum_{c=0}^{C-1} q_{ic} \log\left(p_{ic}\right),
\end{aligned}
\tag{7}
$$

where $q_i \in R^C$ is the one-hot vector of label y_i, i.e., $q_{ic} = \delta\left(y_i, c\right) \in \{0, 1\}$.

Usually, single beat is detected and classified [5]. However, since long signals contain more beats given the sampling rate, prediction on it will be more accurate. In this paper, the length of each sample in the synthetic ECG dataset is 16384 at a sampling rate of 512Hz, which lasts 32s. We split each sample into sub-samples which have the same length of 512. Therefore, each sample contains about ~ 1 beats. It is noteworthy that we do not explicitly extract the beat from the raw signal but use it as the input directly after the Short-Time Fourier Transform. Then, we train our CNN model on this dataset. Besides, to compare the performance of models for longer samples, we also split each sample into sub-samples of different lengths, e.g., 2s, 4s, 8s, 16s. We use

---

[1]Evaluated with FLOPs, i.e., the number of floating-point multiplication-adds.

them to train our CNN models accordingly and denote all these scale-specific models as $h_1 \sim h_6$, respectively. The width of the spectrogram is determined by the length of the wave signal given the window function, which varies for each model. Nevertheless, we use the same architecture for all models and change the pooling strides along columns accordingly while keeping the fully-connected layers fixed.

3.3. Optimization

The optimization of Eq. (7) is not trivial since the objective function $L(\cdot)$ is non-linear and non-convex. Instead of using deterministic optimization methods [32, 33], we adopt the mini-batch Stochastic Gradient Descent (SGD) algorithm [34, 35] in this paper. Mathematically, it can be formulated as:

$$\theta_h^{t+1} = \theta_h^t - \gamma_t \frac{1}{B} \sum_{i=1}^{B} \nabla_{\theta_h} L\left(h\left(s_i, \theta_h\right), y_i\right), \tag{8}$$

where B is the number of training samples in each mini-batch, γ_t is the learning rate at step t. It can be proved that as long as the learning rate γ_t are small enough, the algorithm converges towards a local minimum of the empirical risk [34]. Specifically, to keep the optimization direction and prevent oscillations, we leverage the SGD algorithm with a momentum term [36, 37], $i.e.$,

$$\Delta\theta_h^{t+1} = \alpha\Delta\theta_h^t - \gamma_t \frac{1}{B} \sum_{i=1}^{B} \nabla_{\theta_h} L\left(h\left(s_i, \theta_h\right), y_i\right), \tag{9}$$

and

$$\theta_h^{t+1} = \theta_h^t + \Delta\theta_h^{t+1}, \tag{10}$$

where $\Delta\theta_h$ is the momentum term and α is the momentum parameter. The setting of α, γ, and B will be presented in Section 4.2.1.

3.4. Progressive online decision fusion

For online testing, as the length of signal is growing, we can test it sequentially by using the scale-specific models. As illustrated in Figure 1, lower level models make decisions based on local patterns within short signals, while higher level models make decisions based on global patterns within long signals. These models can be seen as

9

different experts focusing on different scales, whose decisions are complementary and could be fused as a more accurate and stable one [38, 39]. To this end, we propose a progressive online decision fusion method. Mathematically, it can be described as follows:

$$\widetilde{h}\left(x\right) = \sum_{s=1}^{s=s_l} w_s \left(\frac{1}{k_s} \sum_{k=1}^{k=k_s} h_s \left(x^{sk}\right) \right), \tag{11}$$

where $\widetilde{h}\left(\cdot\right)$ represents the fusion result, $s_l \in \{1, 2, 3, 4, 5, 6\}$ is the maximum level for a signal x of specific length. x^{sk} is the kth segment of x for the sth level model h_s, and k_s is the number of segments at s^{th} level, $i.e.$, $k_s = 2^{s_l-s}$. For example, when the length of x is 2048, s_l will be 3, and $k_1 \sim k_3$ will be 4, 2, 1, respectively. w_s is the fusion weight of h_s subjected to $\sum_{s=1}^{s=s_l} w_s = 1$. It can be seen from Eq. (11), decision at each segment at the same level is treated equally. It is reasonable since there is no prior knowledge favouring specific segment and the decision is made by the same model.

Assuming that the distribution of $h_s\left(\cdot\right)$ is independent from each other for any s, with a mean μ_s and variance σ_s, the expectation of Eq. (11) can be derived as:

$$\begin{aligned}
E\left[\widetilde{h}\left(x\right)\right] &= \sum_{s=1}^{s=s_l} w_s \left(\frac{1}{k_s} \sum_{k=1}^{k=k_s} E\left[h_s\left(x^{sk}\right)\right] \right) \\
&= \sum_{s=1}^{s=s_l} w_s \left(\frac{1}{k_s} \sum_{k=1}^{k=k_s} \mu_s \right) \\
&= \sum_{s=1}^{s=s_l} w_s \mu_s.
\end{aligned} \tag{12}$$

For a given training sample x_i, $h_s\left(\cdot\right)$ shares the same training targets y_i. Therefore, μ_s should be the same for any s, denoted as μ. Accordingly, we have the unbiased estimate $E\left[\widetilde{h}\left(x\right)\right] = \mu$. Similarly, we can derive the variance of $\widetilde{h}\left(x\right)$ as: $Var\left[\widetilde{h}\left(x\right)\right] = \sum_{s=1}^{s=s_l} \frac{w_s^2}{k_s}\sigma_s$. Usually, the variance σ_s is decreased with the growth of sample length (scale s) since more "evidence" is accumulated. For instance, if we assume $\sigma_s = \frac{1}{k_s}\sigma$, then we will have $Var\left[\widetilde{h}\left(x\right)\right] = \frac{2^{2s_l+2}-2^2}{2^{2s_l}s_l^2(2^2-1)}\sigma \le \sigma$ for uniform weights $w_s = \frac{1}{s_l}$, and $Var\left[\widetilde{h}\left(x\right)\right] = \frac{2^{4s_l+2}-2^2}{2^{2s_l}(2^{s_l}-1)^2(2^4-1)}\sigma \le \sigma$ for non-uniform weights defined in Eq. (18). Taking $s_l = 6$ as an example, we will have $Var\left[\widetilde{h}\left(x\right)\right] \approx 0.037\sigma$ and $Var\left[\widetilde{h}\left(x\right)\right] \approx 0.2752\sigma$ for uniform and non-uniform weights, respectively. As can be seen, using a fusion decision will reduce the variance and get a more stable result.

4. Experiments

4.1. Evaluation metrics

First, we present the definition of the evaluation metrics used in this paper. Denoting the confusion matrix as $CM = [c_{ij}]$, where c_{ij} is number of samples belonging to the ith category but being predicted as the jth one, the Accuracy, Sensitivity, Specificity and F1 score can be calculated as follows.

$$Accuracy = \sum_{i=1}^{i=C} c_{ii} \bigg/ \sum_{i=1}^{i=C} \sum_{j=1}^{j=C} c_{ij}. \tag{13}$$

$$Sensitivity_i = c_{ii} \bigg/ \sum_{j=1}^{j=C} c_{ij}, \tag{14}$$

where class i represents the symptomatic classes, $e.g.$, RAF, FAF, $etc.$

$$Specificity_k = c_{kk} \bigg/ \sum_{j=1}^{j=C} c_{kj}, \tag{15}$$

where class k represents the normal class.

$$F1_i = 2c_{ii} \bigg/ \left(\sum_{j=1}^{j=C} c_{ij} + \sum_{i=1}^{i=C} c_{ij} \right). \tag{16}$$

$$F1 = \frac{1}{C} \sum_{i=1}^{i=C} F1_i. \tag{17}$$

4.2. Experiments on a synthetic ECG dataset

4.2.1. Dataset and parameter settings

To verify the effectiveness of the proposed method, we construct a synthetic dataset by using an ECG simulator. The simulator can generate different types of ECG signals with different parameter settings. Generally, the ECG signals consist of four types of features, namely, trend, cycle, irregularities, and burst [40]. To cover these

Table 2: Sensitivity and Specificity scores of different methods on the training set. Mean scores and the Standard deviations (mean±std) are reported.

Sensitivity						
Methods	RAF	FAF	AF	SA	AT	ST	PAC
SVM+FFT	0.95±0.02	0.73±0.01	0.77±0.08	**0.77±0.05**	0.85±0.02	0.78±0.10	0.76±0.08
1D CNN [3]	0.96±0.01	0.92±0.04	0.84±0.06	0.39±0.03	0.90±0.01	0.96±0.02	0.20±0.09
Proposed	0.97±0.01	0.99±0.01	0.94±0.01	0.71±0.02	0.94±0.01	0.99±0.01	0.59±0.20
SVM+CNN Feature	**0.98±0.01**	**0.99±0.01**	**0.97±0.01**	0.75±0.01	**0.97±0.01**	**0.99±0.01**	**0.82±0.04**

Sensitivity						
Methods	VB	VTr	PVCCI	VTa	RVF	FVF	AVB-I
SVM+FFT	0.81±0.04	**0.71±0.10**	0.82±0.03	0.84±0.02	0.86±0.03	0.78±0.06	0.82±0.02
1D CNN [3]	0.92±0.03	0.19±0.11	0.87±0.02	0.97±0.01	0.97±0.02	0.96±0.02	0.70±0.17
Proposed	0.93±0.01	0.18±0.19	0.89±0.03	0.99±0.01	0.99±0.01	0.98±0.01	0.77±0.15
SVM+CNN Feature	**0.96±0.01**	0.34±0.12	**0.95±0.01**	**1.00±0.00**	**1.00±0.00**	**0.99±0.01**	**0.95±0.01**

	Sensitivity				Specificity	
Methods	AVB-II	AVB-III	RBBB	LBBB	PVC	N
SVM+FFT	0.84±0.05	0.76±0.07	0.72±0.09	0.81±0.05	**0.76±0.10**	0.86±0.02
1D CNN [3]	0.94±0.03	0.68±0.05	0.91±0.04	0.98±0.01	0.68±0.05	0.95±0.01
Proposed	0.92±0.03	0.86±0.04	0.95±0.01	0.98±0.01	0.72±0.05	0.96±0.01
SVM+CNN Feature	**0.98±0.01**	**0.93±0.03**	**0.97±0.01**	**0.98±0.01**	0.75±0.04	**0.98±0.01**

Table 3: Sensitivity and Specificity scores of different methods on the test set. Mean scores and the Standard deviations (mean±std) are reported.

	Sensitivity						
Methods	RAF	FAF	AF	SA	AT	ST	PAC
SVM+FFT	0.88±0.11	0.44±0.14	0.50±0.21	0.69±0.13	0.53±0.27	0.56±0.21	0.57±0.13
1D CNN [3]	0.96±0.01	0.93±0.04	0.83±0.07	0.38±0.04	0.90±0.02	0.95±0.03	0.20±0.05
Proposed	0.98±0.01	0.99±0.01	0.95±0.03	0.72±0.02	0.94±0.02	0.96±0.03	0.62±0.22
SVM+CNN Feature	0.97±0.01	0.98±0.01	0.96±0.01	0.72±0.02	0.95±0.01	0.96±0.04	0.85±0.03
Proposed(Fusion)	**0.99±0.01**	**1.00±0.00**	**0.99±0.01**	**1.00±0.00**	**1.00±0.00**	**1.00±0.00**	**1.00±0.00**
	Sensitivity						
Methods	VB	VTr	PVCCI	VTa	RVF	FVF	AVB-I
SVM+FFT	0.42±0.29	0.38±0.14	0.54±0.24	0.73±0.09	0.60±0.18	0.45±0.32	0.50±0.30
1D CNN [3]	0.93±0.02	0.15±0.15	0.85±0.03	0.96±0.01	0.96±0.02	0.94±0.04	0.50±0.35
Proposed	0.94±0.01	0.32±0.23	0.91±0.02	0.99±0.01	0.98±0.02	0.99±0.01	0.56±0.30
SVM+CNN Feature	0.96±0.01	0.02±0.02	0.95±0.03	0.98±0.01	0.97±0.02	0.98±0.02	0.48±0.15
Proposed(Fusion)	**1.00±0.00**	**0.99±0.01**	**0.99±0.01**	**1.00±0.00**	**1.00±0.00**	**0.99±0.01**	**0.86±0.20**
	Sensitivity					Specificity	
Methods	AVB-II	AVB-III	RBBB	LBBB	PVC	N	
SVM+FFT	0.66±0.14	0.56±0.21	0.46±0.07	0.48±0.33	0.40±0.24	0.60±0.18	
1D CNN [3]	0.93±0.08	0.64±0.07	0.89±0.10	0.98±0.01	0.69±0.05	0.95±0.02	
Proposed	0.93±0.06	0.87±0.05	0.95±0.02	0.98±0.01	0.57±0.25	0.96±0.02	
SVM+CNN Feature	0.95±0.05	0.89±0.05	0.95±0.02	0.98±0.01	0.57±0.22	0.97±0.02	
Proposed(Fusion)	**1.00±0.00**	**0.95±0.05**	**0.98±0.02**	**1.00±0.00**	**0.99±0.01**	**0.99±0.01**	

features, we choose 20 categories of ECG signals in this paper, which include Normal (N), Rough Atrial Fibrillation (RAF), Fine Atrial Fibrillation (FAF), Atrial Flutter (AF), Sinus Arrhythmia (SA), Atrial Tachycardia (AT), Supraventricular Tachycardia (ST), Premature Atrial Contraction (PAC), Ventricular Bigeminy (VB), Ventricular Trigeminy (VTr), Premature Ventricular Contraction Coupling Interval (PVCCI), Ventricular Tachycardia (VTa), Rough Ventricular Fibrillation (RVF), Fine Ventricular Fibrillation (FVF), Atrio-Ventricular Block I (AVB-I), Atrio-Ventricular Block (AVB-II), Atrio-Ventricular Block (AVB-III), Right Bundle Branch Block (RBBB), Left Bundle Branch Block (LBBB), and Premature Ventricular Contractions (PVC). There are a total of 2426 samples, about 120 samples per category. Each sample has a maximum length of 16384 points sampled at 512Hz. We split the sequence at a random position and merge them by changing their orders. In this way, we augment the dataset and simulate the time delay such that the model can capture the regularity and irregularity in the time series [41]. We use the 3-fold cross-validation to evaluate the proposed method.

Parameters are set as follows. We use the Hamming window of length 256 in Short-Time Fourier Transform and the overlap size is 128. The CNN model is trained in a total of 20,000 iterations with a batch size of 128. The learning rate decreases by half every 5,000 iterations from 0.01 to 6.25×10^{-4}. The momentum and the decay parameter are set to 0.9 and 5×10^{-6}, respectively. We implement the proposed method in CAFFE [42] on a workstation with NVIDIA GTX Titan X GPUs if not specified.

4.2.2. Comparisons with previous methods

We compare the performance of the proposed method with previous methods including SVM based on Fourier transform, the pilot Deep CNN method in [3] which uses 1-D convolutions, and SVM based on the learned features of the proposed method. We report the sensitivity and specificity scores of different methods on both the training set and test set. We also report the average classification accuracy. The standard deviations of each index on the 3-fold cross-validation are also reported. Results are summarized in Table 2, Table 3 and Table 4.

It can be seen that the method in [3] outperforms the traditional method using the

Table 4: Average classification accuracy of different methods on the training set and test test. Standard deviations (Std.) are listed in the brackets.

Methods	Training Set	Test Set
SVM+FFT	0.81($\pm$0.04)	0.56($\pm$0.12)
1D CNN [3]	0.83($\pm$0.01)	0.81($\pm$0.04)
Proposed	0.88($\pm$0.03)	0.87($\pm$0.03)
SVM+CNN Feature	0.93($\pm$0.01)	0.87($\pm$0.02)
Proposed (Fusion)	0.99($\pm$0.01)	**0.99($\pm$0.01)**

FFT coefficients and SVM classifier. However, it is inferior to the proposed one which uses the 2-dimensional spectrogram as input, which benefits from the learned features of time-frequency characteristics. Besides, we use the learned features from the proposed method to train an SVM classifier. The results are denoted as "SVM+CNN Feature". Compared with the SVM with FFT features, the performance of this classifier is significantly boosted. It demonstrates that the proposed method learns a more discriminative feature representation of the ECG signal. Interestingly, it is marginally better than the proposed CNN model which employs a linear classifier. It is reasonable since a more sophisticated nonlinear radial basis kernel is used in the SVM classifier. However, it shows a tendency toward overfitting *i.e.*, a larger gain on the training set.

Moreover, from Table 2 and Table 3, we can find that categories of SA, PAC, VTr, AVB-I, and PVC are hard to be distinguished. We'll shed light on the phenomenon by inspecting the learned features through the visualization technique and analyzing the confusion matrix between categories as follows.

4.2.3. Analysis on learned features and confusion matrix between categories

First, we calculate the learned features from the penultimate layer for all test data. Then, we employ the t-Distributed Stochastic Neighbor Embedding (t-SNE) method proposed in [43, 44] to visually inspect them. The visualization results are shown in Figure 3(a). As can be seen, some categories such as Normal(N), RVF, FVF, ST, RBBB, LBBB, PVCCI, VTa and RAF, are separated from other categories. However, some categories such as SA, PAC, PVC, VTr, AVB-I, and AVB-III, are overlapped
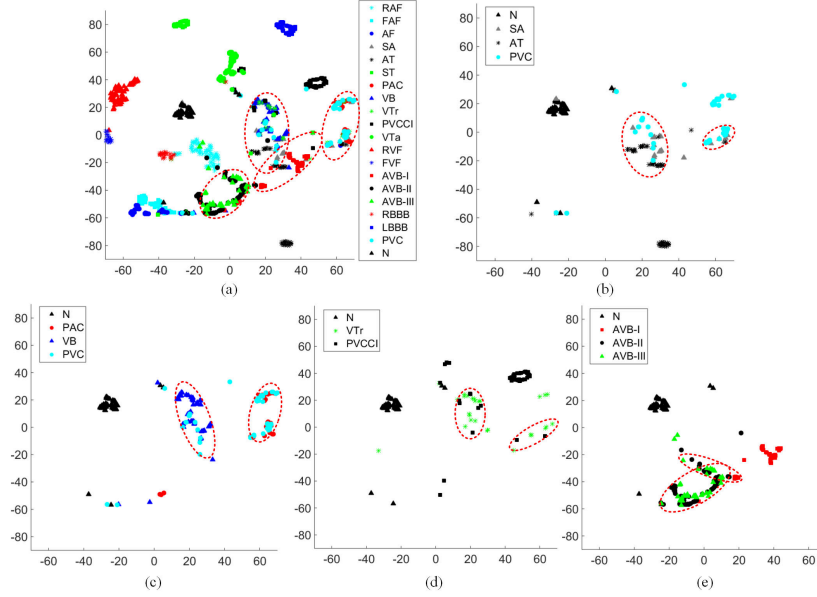
Figure 3: Visualization of the learned features from the proposed network by using t-SNE [43]. (a): Feature clusters of all categories on the test set. (b)-(e): Feature clusters of most confusion categories (denoted by the red circles). Best viewed on screen.

with other categories as indicated by the red circles. We further plot them separately in Figure 3(b)-(e). For example, SA tends to be overlapped with AT and PVC, and PVC tends to be overlapped with PAC and VB. Nevertheless, they are separated from the Normal category, coinciding with the high specificity scores in Table 2 and Table 3.

Besides, we also calculate the confusion matrix of the proposed method at the first level on the test set, which is shown in Figure 4(a). It is clear that some categories are overlapped with others, $e.g.$, SA, VTr, AVB-I, and PVC. The results are consistent with the visual inspection results in Figure 3.

4.2.4. Online decision fusion performance

We test the fusion method in Section 3.4 at different levels s_l: 2, 3, 4, 5, and 6. Two kinds of fusion weights are compared: the uniform one and the one favouring high level models which is calculated as:
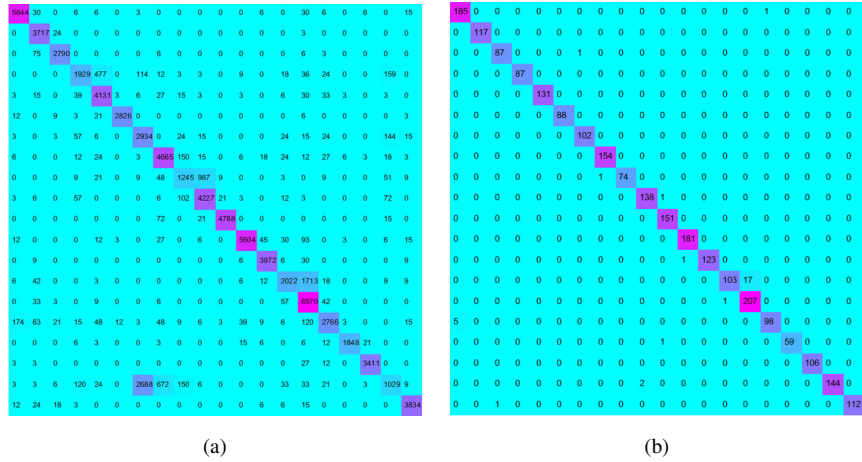
$$w_s = \frac{2^{s-1}}{2^{s_l} - 1}.$$ (18)

16

Figure 4: (a) Confusion matrix of the proposed method at level 1 on the test set. (b) Confusion matrix of the proposed online decision fusion method on the test set. From top to down (top to down), the ground truth (predicted) categories are RAF, FAF, AF, SA, AT, ST, PAC, VB, VTr, PVCCI, VTa, RVF, FVF, AVB-I, AVB-II, AVB-III, RBBB, LBBB, PVC and N, respectively.
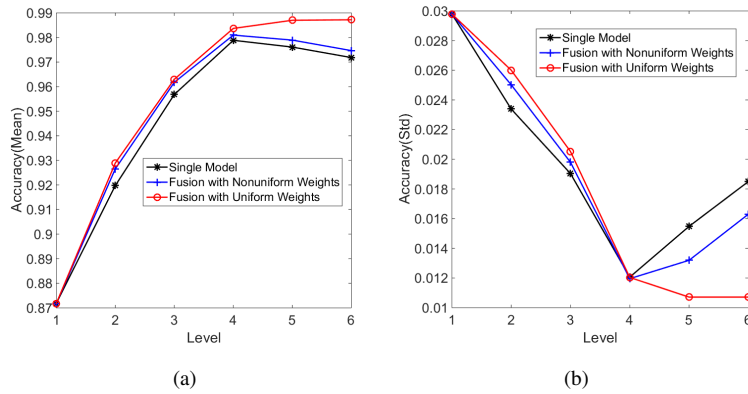

Figure 5: Results of the proposed online decision fusion method. (a) Means of the classification accuracy. (b) Standard deviations (Std) of the classification accuracy.

Figure5 shows the classification accuracy of the proposed fusion method and the proposed single scale method at different levels. First, it can be seen that $h4$ achieves the best performance among all the single models at different levels. The reason may be that it makes a trade-off between data length and the number of model decisions. Compared with $h1$, the input data length is 16 times larger. Compared with $h6$, which only makes a single decision on the whole sequence, $h4$ can make 4 decisions from different scale-specific models and fuse them into a more accurate one.

Then, it can be seen that the fusion results are consistently better than the results of the single-scale model. The performance is improved consistently with the growth of data length. It validates the idea that fusing the complementary decisions from different models leads to a more accurate and stable one. Besides, using non-uniform weights does not provide any advantage over the uniform one. The non-uniform weight strategy favors the higher-level models than the decisions from the lower-level models. Though it is better than the single model, the gains are indeed very marginal. Especially at higher levels, the performance is largely dominated by the model at the highest level. Please refer to Section 3.4 for more details. In conclusion, the proposed online decision fusion method with uniform weights at level 6 achieves the best result. For example, the accuracy is boosted from 87% (single model at level 1) to 99%, and the standard deviation is reduced from 0.03 (single model at level 1) to 0.011. Its sensitivity and specificity scores are shown in Table 3, which shows a significant boost than other methods. The confusion matrix in Figure 4(b) shows the similar results. These results demonstrate the effectiveness of the proposed online decision fusion method.

4.2.5. Computational complexity and running time analysis

We record the running times of the proposed method at GPU and CPU modes, respectively. Results are summarized in Table 5. As can be seen, the running time is only 0.33ms even if it is tested for the whole sequence (level 6). To further examine the computational efficiency of the proposed method, we test it on an NVIDIA Jetson TX2 embedded board. Again, the proposed method can achieve a real-time speed. Interestingly, the running times at GPU mode and CPU mode are comparable. We hypothesize that enlarging the batch size may make full advantage of the GPU acceleration. Af-

Table 5: Running times (millisecond, ms) of the proposed method at different settings.

Device	Titan X		TX2		TX2 (BatchSize: x10)	
Level	GPU	CPU	GPU	CPU	GPU	CPU
1	0.01	0.17	0.17	0.46	0.12	0.44
2	0.03	0.21	0.27	0.59	0.13	0.55
3	0.05	0.26	0.37	0.80	0.14	0.72
4	0.10	0.42	1.22	1.57	0.18	1.39
5	0.21	0.82	2.01	2.91	0.27	2.79
6	0.33	1.33	2.73	5.38	0.56	5.66

ter enlarging the batch size 10 times, the superiority of GPU mode is significant. In conclusion, the proposed method is very efficient and promising to be integrated into a portable ECG monitor with limited computational resources.

4.3. Experiments on a real-world ECG dataset

We also conducted extensive experiments on a real-world ECG dataset used in the 2017 PhysioNet/Computing in Cardiology Challenge [45]. The dataset is split into the training set, validation set, and test set. The training set contains 8,528 single-lead ECG recordings lasting from 9s to 60s. The validation set and test set contain 300 and 3,658 ECG recordings of similar lengths, respectively. The ECG recordings were sampled as 300 Hz. Each sample is labeled into four categories: Normal rhythm, AF rhythm, Other rhythm, and Noisy recordings. Only labels of the training set and validation set are publicly available. Some examples of the ECG waves are shown in Figure 6.

We train our model on the training set. Scores both on the training set and validation set are reported and compared with the top entries in the challenge. It is noteworthy that we add two more convolutional layers after the first and second convolutional layers in the network depicted in Table 1 such that it has a stronger representation capacity to handle the real-world ECG signals better. The number of convolutional filters and kernel sizes are the same as their preceding counterparts. The first fully-connected layer is kept the same. The output number of the last fully-connected layer is modified to be four to keep consistent with the number of categories. Each sample in the dataset
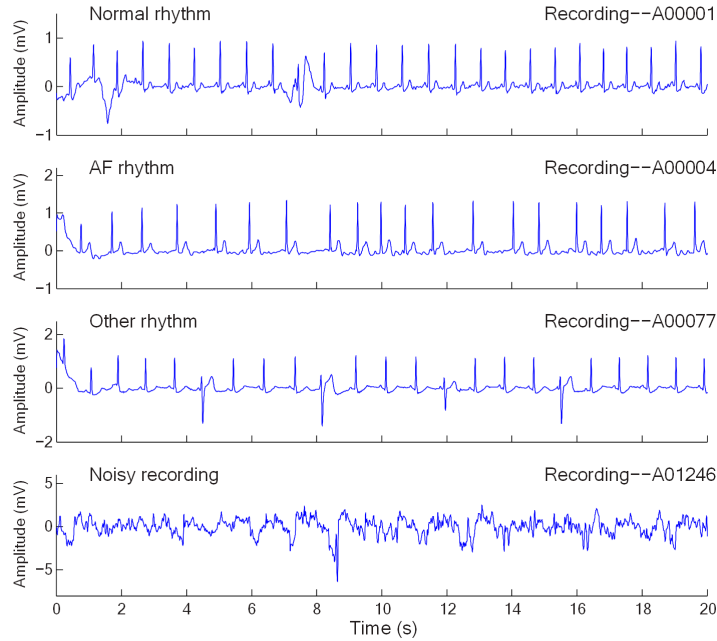
Figure 6: Examples of the ECG waveforms in PhysioNet dataset [45].

is cropped or duplicated to have a length of 16,384. All other hyper-parameters are kept the same as the above experiments if not specified. We train the model at each level three times with random seeds and report the average scores and standard deviations.

4.3.1. Comparisons of the proposed method and the top entries in the challenge

We report the results on this dataset in terms of mean accuracy and F1 score. To keep consistent with the evaluation protocol in [45], we report the average F1 scores for the first three categories. Besides, we also include the average F1 scores for all categories. As can be seen from Figure 7 and Figure 8, the best results are achieved at level 4 ($h4$) and level 5 ($h5$) by the proposed online fusion method, *i.e.*, $100\% \pm 0\%$ classification accuracy and $100\% \pm 0\%$ F1 score. Meanwhile, the results of single models are also competitive. Best results are achieved at level 2 ($h2$) with a $99.44\% \pm 0.57\%$ accuracy and a $99.21\% \pm 0.81\%$ F1 score. It is consistent with the result in Section 4.2.4, where model $h4$ makes a trade-off between data length and the number of model decisions. The comparison results between the proposed method and the top
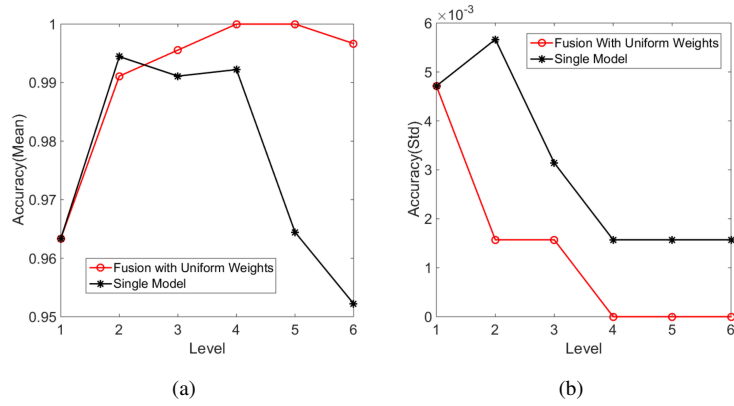
20

(a)   (b)

Figure 7: Results of the proposed online decision fusion method on the PhysioNet dataset [45]. (a) Mean values of the classification accuracy. (b) Standard deviations (Std) of the classification accuracy.
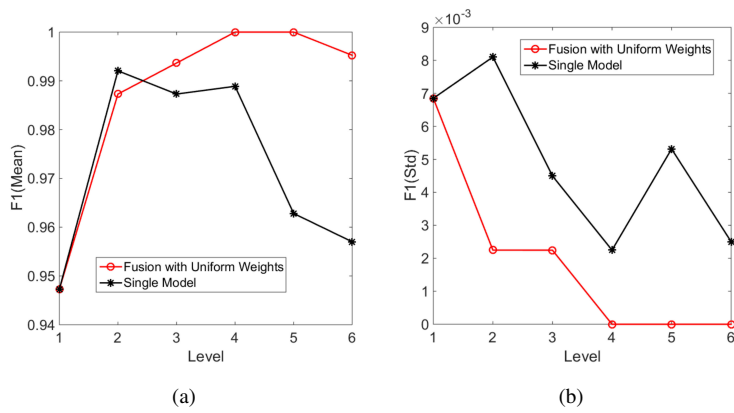

(a)   (b)

Figure 8: Results of the proposed online decision fusion method on the PhysioNet dataset [45]. (a) Mean values of F1 scores. (b) Standard deviations (Std) of the F1 scores.
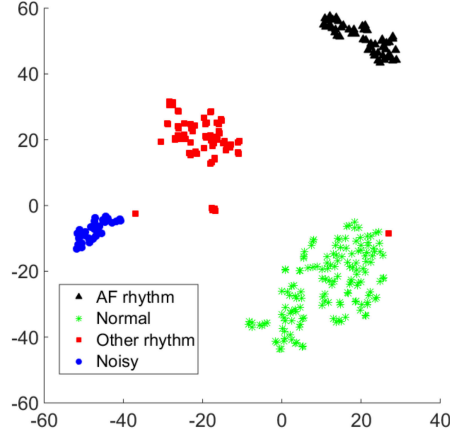
21

Figure 9: Visualization of the learned features from the proposed network on the PhysioNet dataset [45].

entries in the challenge are listed in Table 6. The proposed methods achieve comparable or better results than the top entries on both the training set and validation set.

4.3.2. Analysis on learned features

Similar to Section 4.2.3, we plot the learned features from model $h4$ on the validation set in Figure 9. As can be seen, samples in each category are almost clustered together and separated from other clusters. For several samples in the category of "Other rhythm", they are near the clusters of "Normal" and "Noisy". It implies that these samples are either with noise labels or hard cases which should be carefully handled.

In addition, we plot the spectrograms and their corresponding feature maps from $Conv1$, $Pool1$, $Conv2$ and $Pool2$ layers in Figure 10. As can be seen, the first convolutional layer acts like a basic feature extractor which strengthens the informative parts in the spectrograms. Then, features in low and medium frequencies are pooled and contribute to the final classification. From the $Conv2$ feature maps, we can see that the proposed network generates strong responses in specific frequency zones and accumulate them along the temporal axis. By doing so and together with the online fusion, it learns effective and discriminative features to make an accurate classification.

22

Table 6: Accuracy and F1 scores on the PhysioNet dataset of the proposed methods and the top entries in the challenge. "F1 score" stands for the average F1 score for the first three categories, *i.e.*, Normal rhythm, AF rhythm, and Other rhythm. "F1 score (all categories)" stands for the average F1 score for all categories.

| Rank	Entry	accuracy		F1 score		F1 score (all categories)	
		Validation	Train	Validation	Train	Validation	Train
1	*Teijeiro et al.* [29]	-	-	0.912	0.893	-	-
1	*Datta et al.*	-	-	0.990	0.970	-	-
1	*Zabihi et al.* [28]	-	-	0.968	0.951	-	-
1	*Hong et al.* [27]	-	-	0.990	0.970	-	-
5	*Baydoun et al.*	-	-	0.859	0.965	-	-
5	*Bin et al.*	-	-	0.870	0.875	-	-
5	*Zihlmann et al.*	-	-	0.913	0.889	-	-
5	*Xiong et al.*	-	-	0.905	0.877	-	-
-	*Proposed (level 4)*	0.992±0.002	0.998±0.001	0.989±0.002	**0.996±0.002**	0.992±0.002	0.995±0.003
-	*Proposed (fusion, level 4)*	1.0±0.0	0.999±0.001	**1.0±0.0**	0.994±0.006	1.0±0.0	0.991±0.009

(a)

(b)

(c)

(d)
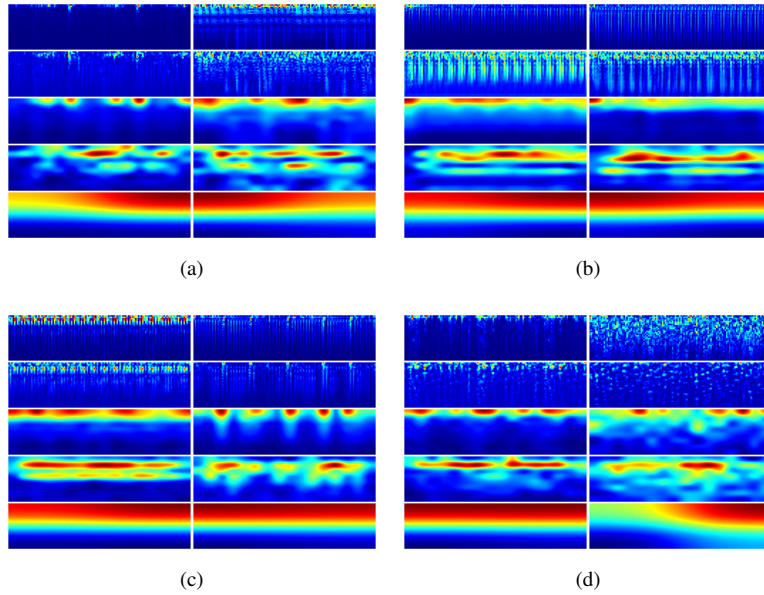
Figure 10: Spectrograms and corresponding feature maps. (a)-(d) shows the results of two samples from AF rhythm, Normal rhythm, Other rhythm, and Noisy rhythm, respectively. In each figure, the spectrograms and corresponding feature maps from $Conv1$, $Pool1$, $Conv2$ and $Pool2$ layers are plotted from the top row to the bottom row, respectively. Hot color represents a strong response.

5. Conclusion and future work

In this paper, we propose a novel deep CNN based method for ECG signal classification. It learns discriminative feature representation from the time-frequency domain by calculating the Short-Time Fourier Transform of the original wave signal. Besides, the proposed online decision fusion method fuses complementary decisions from different scale-specific models into a more accurate one. Extensive experiments on a synthetic 20-category ECG dataset and a real-world AF classification dataset demonstrate its effectiveness. Moreover, the proposed method is computationally efficient and promising to be integrated into a portable ECG monitor with limited computational resources. Future research may include: 1) devising or searching compact and efficient networks to handle complex real-world ECG data; 2) improving the online fusion by integrating both the decisions and learned features at different levels; 3) exploring the potential of the proposed method for nonlinear time series beyond ECG.

References

[1] D. Giri, U. R. Acharya, R. J. Martis, S. V. Sree, T.-C. Lim, T. A. VI, J. S. Suri, Automated diagnosis of coronary artery disease affected patients using lda, pca, ica and discrete wavelet transform, Knowledge-Based Systems 37 (2013) 274–282 (2013). doi:10.1016/j.knosys.2012.08.011.

[2] U. R. Acharya, H. Fujita, V. K. Sudarshan, L. O. Shu, M. Adam, J. E. W. Koh, J. H. Tan, D. N. Ghista, R. J. Martis, C. K. Chua, Automated detection and localization of myocardial infarction using electrocardiogram: a comparative

study of different leads, Knowledge-Based Systems 99 (2016) 146–156 (2016). doi:10.1016/j.knosys.2016.01.040.

[3] S. Kiranyaz, T. Ince, M. Gabbouj, Real-time patient-specific ecg classification by 1-d convolutional neural networks, IEEE Transactions on Biomedical Engineering 63 (3) (2016) 664–675 (2016). doi:10.1109/TBME.2015.2468589.

[4] L.-Y. Shyu, Y.-H. Wu, W. Hu, Using wavelet transform and fuzzy neural network for vpc detection from the holter ecg, IEEE Transactions on Biomedical Engineering 51 (7) (2004) 1269–1273 (2004). doi:10.1109/tbme.2004.824131.

[5] I. Guler, E. D. Ubeyli, Ecg beat classifier designed by combined neural network model, Pattern recognition 38 (2) (2005) 199–208 (2005). doi:10.1016/s0031-3203(04)00276-6.

[6] T. Mar, S. Zaunseder, J. P. Martínez, M. Llamedo, R. Poll, Optimization of ecg classification by means of feature selection, IEEE transactions on Biomedical Engineering 58 (8) (2011) 2168–2177 (2011). doi:10.1109/TBME.2011.2113395.

[7] Y. Wu, R. M. Rangayyan, Y. Zhou, S.-C. Ng, Filtering electrocardiographic signals using an unbiased and normalized adaptive noise reduction system, Medical Engineering & Physics 31 (1) (2009) 17–26 (2009). doi:10.1016/j.medengphy.2008.03.004.

[8] J. Yan, Y. Lu, J. Liu, X. Wu, Y. Xu, Self-adaptive model-based ecg denoising using features extracted by mean shift algorithm, Biomedical Signal Processing and Control 5 (2) (2010) 103–113 (2010). doi:10.1016/j.bspc.2010.01.003.

[9] M. Blanco-Velasco, B. Weng, K. E. Barner, Ecg signal denoising and baseline wander correction based on the empirical mode decomposition, Computers in biology and medicine 38 (1) (2008) 1–13 (2008). doi:10.1016/j.compbiomed.2007.06.003.

[10] V. Bhateja, S. Urooj, R. Mehrotra, R. Verma, A. Lay-Ekuakille, V. D. Verma, A composite wavelets and morphology approach for ecg noise filtering, in: International Conference on Pattern Recognition and Machine Intelligence, Springer, 2013, pp. 361–366 (2013). `doi:10.1007/978-3-642-45062-4_49`.

[11] W. Jenkal, R. Latif, A. Toumanari, A. Dliou, O. El Bcharri, F. M. Maoulainine, An efficient algorithm of ecg signal denoising using the adaptive dual threshold filter and the discrete wavelet transform, Biocybernetics and Biomedical Engineering 36 (3) (2016) 499–508 (2016). `doi:10.1016/j.bbe.2016.04.001`.

[12] S. Poungponsri, X.-H. Yu, An adaptive filtering approach for electrocardiogram (ecg) signal noise reduction using neural networks, Neurocomputing 117 (2013) 206–213 (2013). `doi:10.1016/j.neucom.2013.02.010`.

[13] V. X. Afonso, W. J. Tompkins, T. Q. Nguyen, S. Luo, Ecg beat detection using filter banks, IEEE transactions on biomedical engineering 46 (2) (1999) 192–202 (1999). `doi:10.1109/10.740882`.

[14] N. Zeng, Z. Wang, H. Zhang, Inferring nonlinear lateral flow immunoassay state-space models via an unscented kalman filter, Science China Information Sciences 59 (11) (2016) 112204 (2016). `doi:10.1007/s11432-016-0280-9`.

[15] R. J. Martis, U. R. Acharya, C. M. Lim, J. S. Suri, Characterization of ecg beats from cardiac arrhythmia using discrete cosine transform in pca framework, Knowledge-Based Systems 45 (45) (2013) 76–82 (2013). `doi:10.1016/j.knosys.2013.02.007`.

[16] R. J. Martis, U. R. Acharya, K. Mandana, A. K. Ray, C. Chakraborty, Application of principal component analysis to ecg signals for automated diagnosis of cardiac health, Expert Systems with Applications 39 (14) (2012) 11792–11800 (2012). `doi:10.1016/j.eswa.2012.04.072`.

[17] T. Ince, S. Kiranyaz, M. Gabbouj, A generic and robust system for automated patient-specific classification of ecg signals, IEEE Transactions on Biomedical

Engineering 56 (5) (2009) 1415–1426 (2009). `doi:10.1109/TBME.2009.2013934`.

[18] E. Jayachandran, et al., Analysis of myocardial infarction using discrete wavelet transform, Journal of medical systems 34 (6) (2010) 985–992 (2010). `doi:10.1007/s10916-009-9314-5`.

[19] A. Daamouche, L. Hamami, N. Alajlan, F. Melgani, A wavelet optimization approach for ecg signal classification, Biomedical Signal Processing and Control 7 (4) (2012) 342–349 (2012). `doi:10.1016/j.bspc.2011.07.001`.

[20] M. García, J. Ródenas, R. Alcaraz, J. J. Rieta, Application of the relative wavelet energy to heart rate independent detection of atrial fibrillation, Computer methods and programs in biomedicine 131 (2016) 157–168 (2016). `doi:10.1016/j.cmpb.2016.04.009`.

[21] S. Osowski, L. T. Hoai, T. Markiewicz, Support vector machine-based expert system for reliable heartbeat recognition, IEEE transactions on biomedical engineering 51 (4) (2004) 582–589 (2004). `doi:10.1109/tbme.2004.824138`.

[22] M. Barni, P. Failla, R. Lazzeretti, A.-R. Sadeghi, T. Schneider, Privacy-preserving ecg classification with branching programs and neural networks, IEEE Transactions on Information Forensics and Security 6 (2) (2011) 452–468 (2011). `doi:10.1109/TIFS.2011.2108650`.

[23] J.-S. Wang, W.-C. Chiang, Y.-L. Hsu, Y.-T. C. Yang, Ecg arrhythmia classification using a probabilistic neural network with a feature reduction method, Neurocomputing 116 (2013) 38–45 (2013). `doi:10.1016/j.neucom.2011.10.045`.

[24] A. R. Hassan, M. A. Haque, An expert system for automated identification of obstructive sleep apnea from single-lead ecg using random under sampling boosting, Neurocomputing 235 (2017) 122–130 (2017). `doi:10.1016/j.neucom.2016.12.062`.

[25] J. Oster, G. D. Clifford, Impact of the presence of noise on rr interval-based atrial fibrillation detection, Journal of electrocardiology 48 (6) (2015) 947–951 (2015). `doi:10.1016/j.jelectrocard.2015.08.013`.

[26] Q. Li, C. Liu, J. Oster, G. D. Clifford, Signal processing and feature selection preprocessing for classification in noisy healthcare data, Machine Learning for Healthcare Technologies 2 (2016) 33 (2016). `doi:10.1049/PBHE002E_ch`.

[27] S. Hong, M. Wu, Y. Zhou, Q. Wang, J. Shang, H. Li, J. Xie, Encase: An ensemble classifier for ecg classification using expert features and deep neural networks, in: Computing in Cardiology (CinC), 2017, IEEE, 2017, pp. 1–4 (2017). `doi:10.22489/CinC.2017.178-245`.

[28] M. Zabihi, A. B. Rad, A. K. Katsaggelos, S. Kiranyaz, S. Narkilahti, M. Gabbouj, Detection of atrial fibrillation in ecg hand-held devices using a random forest classifier, in: 2017 Computing in Cardiology (CinC), IEEE, 2017, pp. 1–4 (2017). `doi:10.22489/CinC.2017.069-336`.

[29] T. Teijeiro, C. A. García, D. Castro, P. Félix, Arrhythmia classification from the abductive interpretation of short single-lead ecg records, arXiv preprint arXiv:1711.03892 (2017). `doi:10.22489/CinC.2017.166-054`.

[30] A. S. Ullah, A dna-based computing method for solving control chart pattern recognition problems, CIRP Journal of Manufacturing Science and Technology 3 (4) (2010) 293–303 (2010). `doi:10.1016/j.cirpj.2011.02.002`.

[31] L. Deng, J. Li, J.-T. Huang, K. Yao, D. Yu, F. Seide, M. Seltzer, G. Zweig, X. He, J. Williams, et al., Recent advances in deep learning for speech research at microsoft, in: Acoustics, Speech and Signal Processing (ICASSP), 2013 IEEE International Conference on, IEEE, 2013, pp. 8604–8608 (2013). `doi:10.1109/ICASSP.2013.6639345`.

[32] D. R. Jones, C. D. Perttunen, B. E. Stuckman, Lipschitzian optimization without the lipschitz constant, Journal of optimization Theory and Applications 79 (1) (1993) 157–181 (1993). `doi:10.1007/BF00941892`.

[33] Y. D. Sergeyev, D. Kvasov, M. Mukhametzhanov, On the efficiency of nature-inspired metaheuristics in expensive global optimization with limited budget, Scientific reports 8 (1) (2018) 453 (2018). `doi:10.1038/s41598-017-18940-4.`

[34] L. Bottou, Online learning and stochastic approximations, On-line learning in neural networks 17 (9) (1998) 142 (1998).

[35] L. Bottou, Large-scale machine learning with stochastic gradient descent, in: Proceedings of COMPSTAT'2010, Springer, 2010, pp. 177–186 (2010). `doi:10.1007/978-3-7908-2604-3_16.`

[36] D. E. Rumelhart, G. E. Hinton, R. J. Williams, et al., Learning representations by back-propagating errors, Cognitive modeling 5 (3) (1988) 1 (1988). `doi:10.1038/323533a0.`

[37] I. Sutskever, J. Martens, G. Dahl, G. Hinton, On the importance of initialization and momentum in deep learning, in: International conference on machine learning, 2013, pp. 1139–1147 (2013).

[38] G. Zhang, J. Lu, Y. Gao, Multi-Level Decision Making, Springer, 2015 (2015).

[39] J. Lu, J. Han, Y. Hu, G. Zhang, Multilevel decision-making: A survey, Information Sciences 346 (2016) 463–487 (2016).

[40] A. S. Ullah, Modeling and simulation of complex manufacturing phenomena using sensor signals from the perspective of industry 4.0, Advanced Engineering Informatics 39 (2019) 1–13 (2019). `doi:10.1016/j.aei.2018.11.003.`

[41] A. Sharif Ullah, M. Shamsuzzaman, Fuzzy monte carlo simulation using point-cloud-based probability–possibility transformation, Simulation 89 (7) (2013) 860–875 (2013). `doi:10.1177/0037549713482174.`

[42] Y. Jia, E. Shelhamer, J. Donahue, S. Karayev, J. Long, R. Girshick, S. Guadarrama, T. Darrell, Caffe: Convolutional architecture for fast feature embedding,

in: Proceedings of the 22nd ACM international conference on Multimedia, ACM, 2014, pp. 675–678 (2014). `doi:10.1145/2647868.2654889.`

[43] L. v. d. Maaten, G. Hinton, Visualizing data using t-sne, Journal of machine learning research 9 (Nov) (2008) 2579–2605 (2008).

[44] L. Van Der Maaten, Accelerating t-sne using tree-based algorithms, Journal of machine learning research 15 (1) (2014) 3221–3245 (2014).

[45] G. Clifford, C. Liu, B. Moody, L. Lehman, I. Silva, Q. Li, A. Johnson, R. Mark, Af classification from a short single lead ecg recording: The physionet computing in cardiology challenge 2017, Computing in Cardiology 44 (2017). `doi:10.22489/CinC.2017.065-469.`